2-1-2019

Effects of Rare-Earth (R = Pr, Gd, Ho, Er) Doping on Magnetostructural Phase Transitions and Magnetocaloric Properties in Ni43-xRxMn46Sn11 Shape Memory Alloys

Anil Aryal
Southern Illinois University Carbondale

Sudip Pandey
Southern Illinois University Carbondale

Igor Dubenko
Southern Illinois University Carbondale

Dipanjan Mazumdar
Southern Illinois University Carbondale

Shane Stadler
Louisiana State University

See next page for additional authors

Recommended Citation

Aryal, A., Pandey, S., Dubenko, I., Mazumdar, D., Stadler, S., & Ali, N. (2019). Effects of Rare-Earth (R = Pr, Gd, Ho, Er) Doping on Magnetostructural Phase Transitions and Magnetocaloric Properties in Ni43-xRxMn46Sn11 Shape Memory Alloys. *IEEE Transactions on Magnetics, 55* (2) https://doi.org/10.1109/TMAG.2018.2868134

Effects of Rare-Earth (R = Pr, Gd, Ho, Er) Doping on Magnetostructural Phase Transitions and Magnetocaloric Properties in $Ni_{43-x}R_xMn_{46}Sn_{11}$ Shape Memory Alloys

Anil Aryal[1], Sudip Pandey[1], Igor Dubenko[1], Dipanjan Mazumdar[1], Shane Stadler[2], and Naushad Ali[1]

[1]Department of Physics, Southern Illinois University, Carbondale, IL 62901 USA
[2]Department of Physics & Astronomy, Louisiana State University, Baton Rouge, LA 70803 USA

A series of rare-earth-doped $Ni_{43-x}R_xMn_{46}Sn_{11}$ (x = 0, 1 and R = Pr, Gd, Ho, Er) alloys was fabricated by arc melting, and their structural, magnetic, and magnetocaloric properties were studied through room temperature X-ray diffraction (XRD), differential scanning calorimetry, and magnetization measurements. Analysis of XRD data reveal that the alloys crystallize in the cubic $L2_1$ austenite phase structure as the major phase with a small trace of martensitic phase (MP). The martensitic transition temperature (T_M) shifts to consecutive higher temperatures with the substitution of Pr, Gd, Ho, and Er. A drastic shift in T_M by ∼60 K relative to the parent compound (T_M = 195 K) was found for $Ni_{42}PrMn_{46}Sn_{11}$. Large values of magnetic entropy changes (ΔS_M) of 32 (Pr), 28 (Gd), and 25 J · kg^{-1} · K^{-1} (Ho) were obtained at T_M for ΔH = 50 kOe. A maximum value of the refrigeration capacity of ∼250 J · kg^{-1} was obtained in the vicinity of T_M for ΔH = 50 kOe for the Ho-doped compound. A large exchange bias effect with H_{EB} ∼ 1.1 kOe at 10 K was observed for the Pr-doped compound in its MP.

Index Terms—**Exchange bias, magnetocaloric, magnetoresistance, magnetostructural transitions, rare-earth doped Heusler alloys.**

I. Introduction

THE magnetocaloric effect (MCE) is an adiabatic temperature change (ΔT_A) or isothermal magnetic entropy change (ΔS_M) in a magnetic material, induced by an applied magnetic field. The MCE has been a subject of intense investigation due to its potential application in magnetic refrigeration, a solid-state cooling technology that is environmentally friendly and efficient compared to the traditional gas compressed refrigerators [1], [2]. However, the successful development of this technology requires the discovery of new materials that are less expensive and show large MCE values near room temperature. Extensive research is being conducted on some material systems that undergo the first-order magnetostructural transitions (MSTs) and show giant MCEs. Such materials include as $Gd_5Si_2Ge_2$, MnFe(P, As), $LaFe_{13-x}Si_x$, $MnAs_{1-x}Sb_x$, and NiMnX (X = Ga, Sn, Sb, In) Heusler alloys [3]–[11].

Recently, off-stoichiometric Ni-Mn-X (X = In, Sn, Sb)-based Heusler alloys have attracted attention because they undergo a first-order martensitic transitions (MTs) from a high symmetry (cubic $L2_1$-type) austenite phase (AP) to a low symmetry (10 M, 14 M, or $L1_0$) martensitic phase (MP) [7], [8], [11]. These alloys show remarkable magnetoresponsive properties such as magnetic shape memory effects, exchange bias (EB), large magnetoresistance (MR), and large MCEs [7], [9], [12]–[18] associated with the MT. It has been reported that the MT temperatures in these alloys can be tuned by changing the chemical composition of the alloy, or by the doping of extra elements. The valance electron concentration per atom and the distance between the Mn–Mn atoms are considered as the major factor affecting the structural and magnetic properties of the Ni–Mn–X-based Heusler alloys [8], [11], [19]. These factors can modify the electronic band structure and affect the phase transitions and associated phenomena [11]. However, the exact mechanisms responsible for the unique behaviors shown by these alloys are not clear. Thus, studies of the influence of doping on the physical properties can provide new information important for understanding their behaviors, and applicability in new technological areas. The magnetic rare-earth (RE) atoms are characterized by magnetic moments originating from 4f electronic atomic shell. The 4f electrons reside in an internal atomic shell and do not directly hybridize with conduction electrons. Thus, RE ions are characterized by large and localized magnetic moments (up to 10 μ_B/atom for Dy^{+3}) and strong spin-orbit coupling. The introduction of the RE ions into Heusler alloys can, therefore, facilitate the study of the effect of above-mentioned factors on their functional properties.

To date, reports on the effect of RE element doping in NiMn-based Heusler alloys are limited. In this paper, we present the results of doping RE elements (R = Pr, Gd, Ho, and Er) in the $Ni_{43-x}R_xMn_{46}Sn_{11}$($x$ = 0, 1) Heusler system and its effect on the phase transitions, magnetic entropy changes, and functional properties such as shape memory effects, EB, MR, and MCE related to MT.

II. Experimental Techniques

Approximately 4g polycrystalline samples with nominal compositions were fabricated by arc-melting high-purity elements (99.99%) in an ultra-high purity argon atmosphere. The details of sample synthesis procedures and the handling of RE metals are published elsewhere [20]. The ingots were then wrapped in tantalum foil and annealed in high vacuum (∼10^{-4}

Manuscript received May 28, 2018; revised August 3, 2018; accepted August 29, 2018. Date of publication September 26, 2018; date of current version January 18, 2019. Corresponding author: A. Aryal (e-mail: aryalanil@siu.edu).

Digital Object Identifier 10.1109/TMAG.2018.2868134

torr) for 48 h at 850 °C, and then slowly cooled to room temperature. The phase purity and crystal structures were obtained using a high-resolution Rigaku SmartLab X-ray diffractometer using CuK_α radiation at room temperature. The magnetization and resistivity (four-probe method) were measured using a SQUID magnetometer (quantum design) in the temperature interval 5–380 K, and in applied magnetic fields up to 50 kOe. Magnetic measurements were taken following the protocols: the samples were first cooled from 400 to 10 K at zero field. The zero-field-cooling (ZFC) measurements were then carried out while heating the samples to 400 K in an applied magnetic field, and followed by the field-cooled-cooling (FCC) measurement to 10 K. Finally, the field-cooled-heating (FCH) measurement was made from 10 to 400 K. The phase transition temperatures were determined from the minimum of the dM/dT versus T curves (from $M(T)$ data) during the heating cycle. Differential scanning calorimetry (DSC) measurements were carried out using a DSC 8000 instrument (PerkinElmer) with a ramp rate of 20 K/min during heating and cooling, and in the temperature range of 123–423 K. The latent heat (L) was estimated from the endothermic peaks of the heat flow curves using the equation, $L = \int_{T_s}^{T_f} (dQ/dT)dT$, where (dQ/dT) is the change in heat flow with respect to temperature, and T_s and T_f are the initial and final temperatures of the structural phase transition on heating, respectively. The total entropy changes (ΔS_T) were calculated using $\Delta S_T = L/T_M$, where L is the latent heat in $J \cdot kg^{-1}$ and T_M is the MT temperature in K corresponding to the peak position in the DSC heat flow curves.

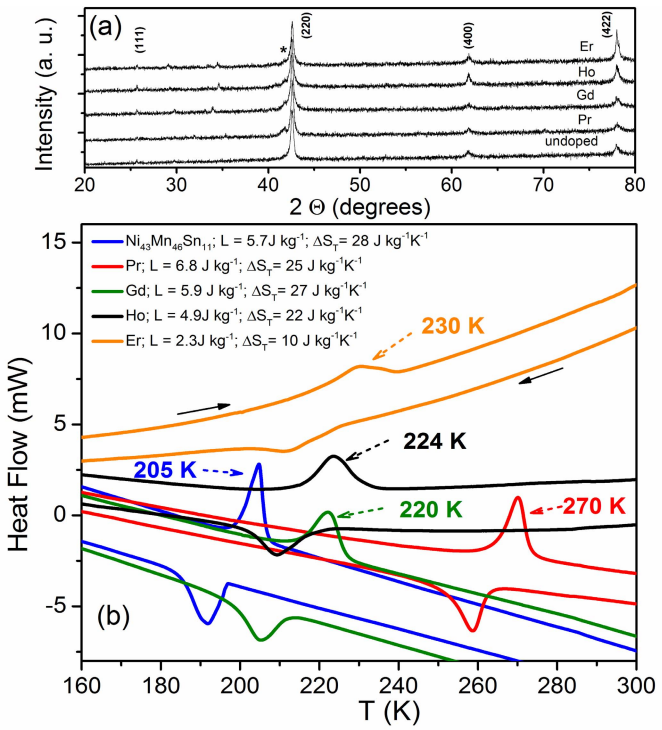

Fig. 1. (a) Room temperature XRD patterns of $Ni_{43}Mn_{46}Sn_{11}$ and the RE-doped $Ni_{42}RMn_{46}Sn_{11}$(R = Pr, Gd, Ho, Er) alloys of nominal compositions. The XRD peaks of the cubic AP are indexed. The symbol "∗" represents the peak from the MP. (b) DSC heat flow curves as a function of temperature. The solid arrows indicate the heating and cooling cycles.

III. Results and Discussion

Fig. 1(a) shows the room temperature X-ray diffraction (XRD) patterns of the parent $Ni_{43}Mn_{46}Sn_{11}$ and the RE-doped $Ni_{42}RMn_{46}Sn_{11}$(R = Pr, Gd, Ho, Er) alloys. The diffraction peaks observed for all samples at room temperature can be identified as belonging to the cubic $L2_1$ austenitic as the main phase. However, a small trace of the MP, and some unknown phases, is also visible for the RE-doped alloys. The XRD pattern has been indexed with the Miller indices of the cubic $L2_1$ structure.

The occurrence of the first-order MT in the alloys was examined using DSC measurements as shown in Fig. 1(b). A transition from MP/AP to AP/MP with large endothermic/exothermic peaks with thermal hysteresis was observed in the heat flow curves during the heating/cooling cycles. The observed peaks arise from the latent heat of the structural transition. The values of T_M, latent heat (L), and the total entropy change (ΔS_T) associated with MTs were determined and are summarized in Fig. 1(b). The MT temperature was found to increase relative to the undoped $Ni_{43}Mn_{46}Sn_{11}$ alloy with corresponding doping of heavy RE elements Gd, Ho, and Er. Interestingly, for the Pr (light RE)-doped alloy, a drastic shift in T_M(∼65 K) to 270 K relative to the undoped compound was observed. Thus, doping small amount of RE elements in $Ni_{43}Mn_{46}Sn_{11}$ Heusler alloys increases the stability of the MP at higher temperatures.

Fig. 2(a)–(e) and (f) shows the $M(T)$ curves of the alloys in applied fields of 100 Oe and 50 kOe, respectively. The FCC and FCH $M(T)$ curves at $H = 100$ Oe for the parent $Ni_{43}Mn_{46}Sn_{11}$ show that the compound is in a ferromagnetic (FM) state in both the MP and AP. As the temperature increases, three successive magnetic transitions are observed: 1) FM to low-magnetic martensitic phase (LMMP) at T_C^M; 2) from LMMP to a ferromagnetic austenite phase (FMAP) at the MST ($T_M \sim 195$ K); and 3) from an FMAP to a paramagnetic AP at (T_C^A). A temperature hysteresis in the $M(T)$ curves on heating (FCH) and cooling (FCC) clearly indicates a first-order structural transition from the MP to AP. The $M(T)$ curves for the doped alloys evolve in similar manner to that of the parent alloy as shown in Fig. 2(b)–(e). However, the effect of doping can be seen in T_M. T_M shifts progressively to higher temperatures with the corresponding substitutions of Pr, Gd, Ho, and Er [see Fig. 2(a)–(e) for values], with a maximum shift of ∼60 K for $Ni_{42}PrMn_{46}Sn_{11}$ alloy at $H = 100$ Oe. The T_M from the magnetization measurements showed a similar tendency as that observed in the DSC measurement of all of the alloys. An interesting feature observed in the $M(T)$ curves [Fig. 2(b)–(e)], typical of off-stoichiometric Ni–Mn–X (X = In, Sn, Sb) Heusler alloys, is the splitting of the ZFC and FCC curves at temperatures below T_C^M. This type of splitting is related to magnetic inhomogeneity and results in an EB effect [7], [17].

The magnetic entropy changes (ΔS_M) of all alloys near the characteristic temperatures (T_M and T_C) were calculated from the isothermal $M(H)$ curves using Maxwell's relation, $\Delta S_M = \int_0^H ((\partial M/\partial T))_H dH$, and are shown in Fig. 3. Both

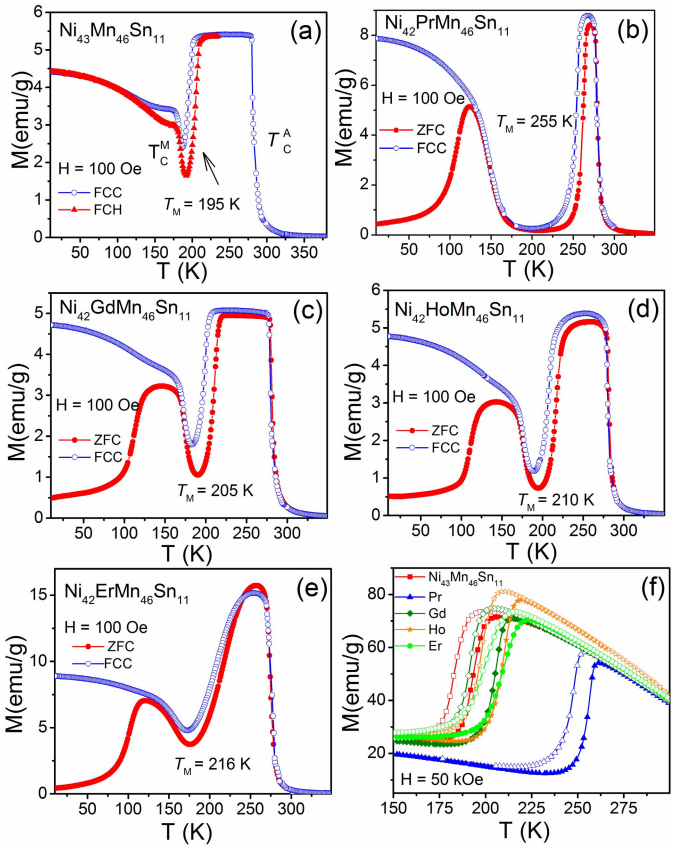

Fig. 2. Temperature dependence of the magnetization $M(T)$ of $Ni_{43}Mn_{46}Sn_{11}$ and $Ni_{42}RMn_{46}Sn_{11}$(R = Pr, Gd, Ho, Er) alloys on heating and cooling in an applied magnetic field of (a)–(e) 100 Oe and (f) 50 kOe. The solid and open symbols represent the ZFC/FCH and FCC cycles, respectively.

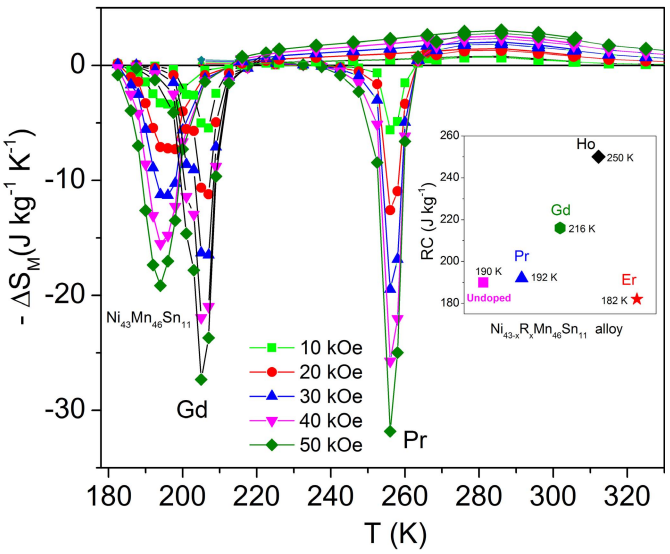

Fig. 3. Magnetic entropy changes $(-\Delta S_M)$ as a function of temperature for the parent and RE-doped alloys near T_M and T_C^A with a magnetic field change $\Delta H = 50$ kOe. For clarity, only $-\Delta S_M$ curves for the parent, Pr-, and Gd-doped alloys are shown. Inset: RC values for the parent and RE-doped alloys with $\Delta H = 50$ kOe.

direct (with negative ΔS_M values at T_C) and inverse (with positive ΔS_M values at T_M) MCEs were observed for all alloys. Maximum entropy changes of about 32, 28, 25, and 14 $J \cdot kg^{-1} \cdot K^{-1}$ have been observed at T_M for the compounds doped with Pr, Gd, Ho, and Er, respectively, for a field change of 50 kOe. The large values of ΔS_M originate from the sharp change in magnetization during MTs. Furthermore, since the peaks of the $\Delta S_M(T)$ curves shift toward higher temperatures with RE doping, large inverse MCEs can be obtained in a wide temperature ranges, from 195 to 255 K in this case, which is important for applications.

From the $\Delta S_M(T)$ curves, an important parameter known as the refrigeration capacity (RC) has been calculated using the formula: $|(\Delta S_M)_{\text{peak}}| \times \delta T_{\text{FWHM}}$, where $\delta T_{\text{FWHM}} = T_{\text{hot}} - T_{\text{cold}}$ are the temperatures that define the full-width at half-maximum of $\Delta S_M(T)$ [21]. The RC is a measure of the amount of heat transferred between the hot and cold reservoirs in an ideal refrigeration cycle. Large RC values were observed with a maximum of 250 $J \cdot kg^{-1}$ for the Ho-doped alloy at T_M with $\Delta H = 50$ kOe. As shown in the inset of Fig. 3, the RC is enhanced by RE doping except for the Er-doped alloy due to its lower ΔS_M value. Interestingly for the Pr-doped alloy (with the maximum ΔS_M value), the RC value is slightly greater than that of the parent compound (190 $J \cdot kg^{-1}$) because of the decrease in peak width of ΔS_M curve. The large values of the RC observed at the MST illustrate the potential use of these alloys as working materials for magnetic refrigeration.

In order to understand the magnetic behavior of the samples at low temperature, we studied the EB effect, a phenomenon often observed in NiMn-based Heusler alloys. The EB effect is a shift in the center of the hysteresis loop from zero magnetic field. This phenomenon results from the exchange interaction between FM and antiferromagnetic fractions of the alloys. Fig. 4(a) shows the low-temperature magnetization isotherm loop of the parent $Ni_{43}Mn_{46}Sn_{11}$ and the Pr- and Gd-doped alloys. The $M(H)$ isotherms were obtained after the samples were cooled down to 10 K at $H = 500$ Oe. A shift in the hysteresis loop from the origin in the $M(H)$ isotherms, i.e., an EB was observed in the alloys. The observed EB effect is a clear indication of the magnetic inhomogeneity in these alloys, further supporting the observed splitting of the $M(T)$ (ZFC, FCC) curves at low temperature. A large EB field (H_{EB}) of 770 Oe was observed in the parent alloy. Much larger H_{EB} values of 1100, 905, and 942 Oe were found for the Pr-, Gd-, and Er-doped alloys, respectively. The maximum H_{EB}, obtained for the Pr-doped alloy, is comparable to the largest value reported for Ni–Mn–Sn-based Heusler system (1170 Oe, FC = 500 Oe) [18]. The large EB effect possessed by these RE-doped alloys has possible applications in permanent magnets, magnetic recording media, sensors, and magnetic read heads [17].

The temperature dependence of the resistivity (ρ) in 0 and 50 kOe applied fields near T_M was studied for the alloy-doped with Gd and is shown in Fig. 4(b). As can be seen from the $\rho(T)$ curve, the alloy shows high resistivity in the MP, which drops sharply at T_M to a much smaller value in the AP. The observed variation in ρ between the MP and AP of the alloy can be explained on the basis of the density

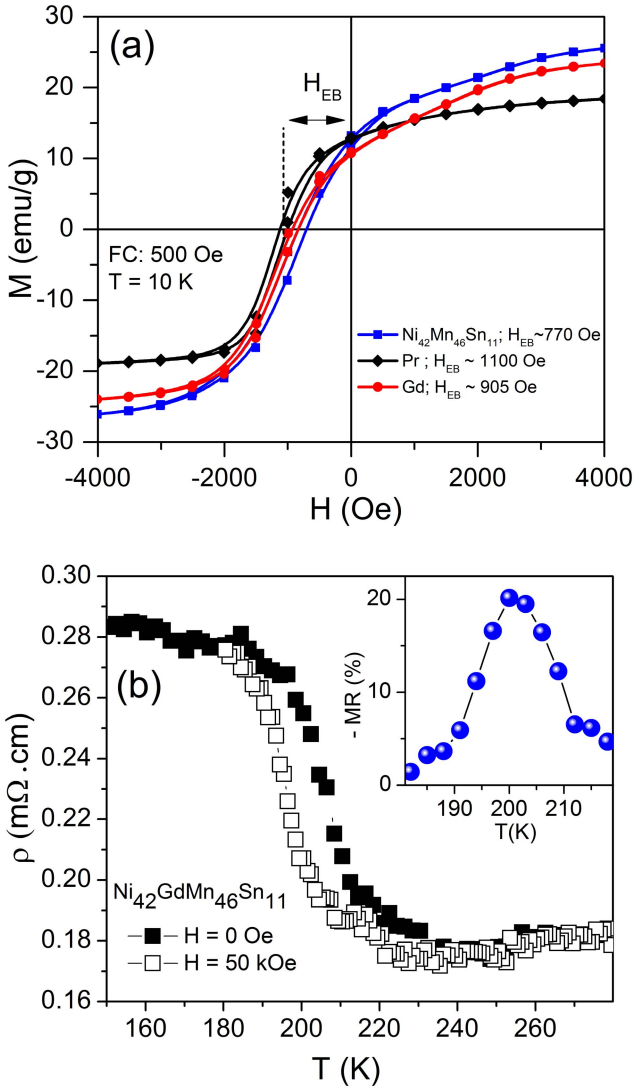

Fig. 4. (a) $M(H)$ loops of $Ni_{43}Mn_{46}Sn_{11}$ and the Pr- and Gd-doped alloys measured after the samples were cooled to 10 K in a applied field of $H =$ 500 Oe. (b) Resistivity (ρ) as a function of temperature (T) at $H = 0$ and 50 kOe for the Gd-doped alloy. Inset: MR as a function of T.

of electronic states at the Fermi energy, $N(E_F)$, according to the relationship, $\rho \sim [N(E_F)]^{-2}$ [11]. Since $N(E_F)$ in the MP is smaller than in the AP, its value of ρ will be larger. From the $\rho(T)$ curve, the MR as a function of T was estimated for a field change of 50 kOe [see inset of Fig. 4(b)]. The MR is defined as $\text{MR}(\%) = (\Delta\rho/\rho_o) \times 100\%$, where $\Delta\rho = [\rho(H, T) - \rho_o]$ and $\rho_o = \rho(H = 0, T)$. Significant MR values reaching -20% were found for the $Ni_{42}GdMn_{46}Sn_{11}$ alloy for a magnetic field change of 50 kOe near T_M. The magnetotransport measurements in NiMn-based Heusler alloys are interesting from both fundamental science and application points of view. The MR measurements provide important information about phase-transformations, electronic structure, and scattering mechanisms in these high-resistivity FM Heusler alloys [11]. From an application point of view, materials with giant MR values can be utilized in technological devices such as magnetic field sensors and hard-disk read heads [22]–[25].

IV. Conclusion

The structural, magnetic, magnetocaloric, and transport properties of $Ni_{43}Mn_{46}Sn_{11}$ and $Ni_{42}RMn_{46}Sn_{11}$ (R = Pr, Gd, Ho, and Er) alloys have been investigated. The results indicate that: 1) the alloys predominantly crystallize in the cubic $L2_1$ AP as main phase at room temperature with a small trace of MP; 2) T_M shifts towards higher temperature with a maximum shift of ~60 K with RE doping, thus stabilizing the MP at higher temperature; 3) large values of MCE parameters ΔS_M and RC were found that can be tuned in a wide temperature range (195–255 K); 4) a large H_{EB} was observed indicating a magnetic inhomogeneity of the MP; and 5) the alloy shows significant MR values at T_M. Thus, the pronounced multifunctional properties such as FM shape memory effects, MCE, EB, and MR of the RE-doped $Ni_{43-x}R_xMn_{46}Sn_{11}$ Heusler alloys make this system promising for the ongoing development of magnetocaloric and multifunctional technologies.

Acknowledgment

This work was supported by the U.S. Department of Energy, Office of Science, Basic Energy Sciences under Grant DE-FG02-06ER46291 (SIU) and Grant DE-FG02-13ER46946 (LSU).

References

[1] K. A. Gschneidner, Jr., V. K. Pecharsky, and A. O. Tsokol, "Recent developments in magnetocaloric materials," *Rep. Prog. Phys.*, vol. 68, no. 6, p. 1479, 2005.
[2] A. M. Tishin and Y. I. Spichkin, *The Magnetocaloric Effect and Its Applications*. London, U.K.: Institute of Physics, 2003.
[3] V. K. Pecharsky and K. A. Gschneidner, Jr., "Giant magnetocaloric effect in $Gd_5(Si_2Ge_2)$," *Phys. Rev. Lett.*, vol. 78, p. 4494, Jun. 1997.
[4] O. Tegus, E. Brück, K. H. J. Buschow, and F. R. de Boer, "Transition-metal-based magnetic refrigerants for room-temperature applications," *Nature*, vol. 415, pp. 150–152, Jan. 2002.
[5] A. Fujita, S. Fujieda, Y. Hasegawa, and K. Fukamichi, "Itinerant-electron metamagnetic transition and large magnetocaloric effects in $La(Fe_xSi_{1-x})_{13}$ compounds and their hydrides," *Phys. Rev. B, Condens. Matter*, vol. 67, p. 104416, Mar. 2003.
[6] H. Wada and Y. Tanabe, "Giant magnetocaloric effect of $MnAs_{1-x}Sb_x$," *Appl. Phys. Lett.*, vol. 79, pp. 3302–3304, Sep. 2001.
[7] I. Dubenko, M. Khan, A. K. Pathak, B. R. Gautam, S. Stadler, and N. Ali, "Magnetocaloric effects in Ni–Mn–X based Heusler alloys with X=Ga, Sb, In," *J. Magn. Magn. Mater.*, vol. 321, pp. 754–757, Apr. 2009.
[8] T. Krenke, M. Acet, E. F. Wassermann, X. Moya, L. Mañosa, and A. Planes, "Martensitic transitions and the nature of ferromagnetism in the austenitic and martensitic states of Ni-Mn-Sn alloys," *Phys. Rev. B, Condens. Matter*, vol. 72, p. 014412, Jul. 2005.
[9] T. Krenke *et al.*, "Inverse magnetocaloric effect in ferromagnetic Ni–Mn–Sn alloys," *Nature Mater.*, vol. 4, no. 6, p. 450, 2005.
[10] F.-X. Hu, B.-G. Sen, and J.-R. Sun, "Magnetic entropy change in $Ni_{51.5}Mn_{22.7}Ga_{25.8}$ alloy," *Appl. Phys. Lett.*, vol. 76, pp. 3460–3462, Apr. 2000.
[11] I. Dubenko *et al.*, "Magnetic, magnetocaloric, magnetotransport, and magneto-optical properties of Ni–Mn–In-based Heusler alloys: Bulk, ribbons, and microwires," in *Novel Functional Magnetic Materials* (Springer Series in Materials Science). Cham, Switzerland: Springer, 2016, pp. 41–82.
[12] Y. Sutou *et al.*, "Magnetic and martensitic transformations of NiMnX (X = In, Sn, Sb) ferromagnetic shape memory alloys," *Appl. Phys. Lett.*, vol. 85, pp. 4358–4360, Sep. 2004.

[13] R. Kainuma *et al.*, "Magnetic-field-induced shape recovery by reverse phase transformation," *Nature*, vol. 439, p. 957, Feb. 2006.
[14] I. Dubenko *et al.*, "Giant Hall effect in Ni-Mn-In Heusler alloys," *Phys. Rev. B, Condens. Matter*, vol. 80, p. 092408, Sep. 2009.
[15] A. K. Pathak, M. Khan, I. Dubenko, S. Stadler, and N. Ali, "Large magnetic entropy change in $Ni_{50}Mn_{50-x}In_x$ Heusler alloys," *Appl. Phys. Lett.*, vol. 90, p. 262504, May 2007.
[16] M. Khan, A. K. Pathak, M. R. Paudel, I. Dubenko, S. Stadler, and N. Ali, "Magnetoresistance and field-induced structural transitions in $Ni_{50}Mn_{50-x}Sn_x$ Heusler alloys," *J. Magn. Magn. Mater.*, vol. 320, pp. L21–L25, Feb. 2008.
[17] M. Khan, I. Dubenko, S. Stadler, and N. Ali, "Exchange bias in bulk Mn rich Ni–Mn–Sn Heusler alloys," *J. Appl. Phys.*, vol. 102, no. 11, p. 113914, 2007.
[18] L. Ma *et al.*, "Coexistence of reentrant-spin-glass and ferromagnetic martensitic phases in the $Mn_2Ni_{1.6}Sn_{0.4}$ Heusler alloy," *Appl. Phys. Lett.*, vol. 99, no. 18, p. 182507, 2011.
[19] M. Khan, I. Dubenko, S. Stadler, and N. Ali, "Magnetic and structural phase transitions in Heusler type alloys $Ni_2MnGa_{1-x}In_x$," *J. Phys., Condens. Matter*, vol. 16, p. 5259, Jul. 2004.
[20] A. Aryal, A. Quetz, S. Pandey, I. Dubenko, S. Stadler, and N. Ali, "Magnetocaloric effects and transport properties of rare-Earth (R = La, Pr, Sm) doped $Ni_{50-x}R_xMn_{35}Sn_{15}$ Heusler alloys," *J. Alloys Compounds*, vol. 717, pp. 254–259, Sep. 2017.
[21] A. Aryal *et al.*, "Large reversible magnetic entropy change in rapidly solidified $Ni_{0.895}Cr_{0.105}MnGe_{1.05}$ melt-spun ribbons," *Intermetallics*, vol. 97, pp. 89–94, Jun. 2018.
[22] U. Hartmann, Ed., *Magnetic Multilayers and Giant Magnetoresistance: Fundamentals and Industrial Applications*. Berlin, Germany: Springer-Verlag, 2000.
[23] V. D. Krishna, K. Wu, A. M. Perez, and J.-P. Wang, "Giant magnetoresistance-based biosensor for detection of influenza a virus," *Frontiers Microbiol.*, vol. 7, p. 400, Mar. 2016.
[24] C. Giebeler, T. Kuiper, J. B. A. D. van Zon, M. Doescher, G. Schulz, and D. Oelgeschlaeger, "Robust GMR sensors for automotive applications," *Tech. Meas. Platform Methods, Syst. Appl. Metrol.*, vol. 68, no. 5, p. 215, 2001.
[25] D. R. Baselt, G. U. Lee, M. Natesan, S. W. Metzger, P. E. Sheehan, and R. J. Coltona, "A biosensor based on magnetoresistance technology," *Biosensors Bioelectron.*, vol. 13, pp. 731–739, Oct. 1998.